European Journal of Medicinal Chemistry 172 (2019) 16–25

Contents lists available at ScienceDirect

European Journal of Medicinal Chemistry

journal homepage: http://www.elsevier.com/locate/ejmech

Research paper

Targeting gliomas with triazene-based hybrids: Structure-activity relationship, mechanistic study and stability

Cláudia Braga [a], Ana R. Vaz [a], M. Conceição Oliveira [b], M. Matilde Marques [b], Rui Moreira [a], Dora Brites [a], Maria J. Perry [a, *]

[a] Research Institute for Medicines (iMed.ULisboa), Faculdade de Farmácia, Universidade de Lisboa, Av. Professor Gama Pinto, 1649-003 Lisboa, Portugal
[b] Centro de Química Estrutural, Instituto Superior Técnico, Universidade de Lisboa, Av. Rovisco Pais, 1049-001 Lisboa, Portugal

ARTICLE INFO

Article history:
Received 28 January 2019
Received in revised form
18 March 2019
Accepted 19 March 2019
Available online 22 March 2019

Keywords:
Triazenes
Histone deacetylase inhibitors
Valproic acid
Multi-targeted glioma therapy

ABSTRACT

Herein we report novel hybrid compounds based on valproic acid and DNA-alkylating triazene moieties, **1**, with therapeutic potential for glioblastoma multiforme chemotherapy. We identified hybrid compounds **1d** and **1e** to be remarkably more potent against glioma and more efficient in decreasing invasive cell properties than temozolomide and endowed with chemical and plasma stability. In contrast to temozolomide, which undergoes hydrolysis to release an alkylating metabolite, the valproate hybrids showed a low potential to alkylate DNA. Key physicochemical properties align for optimal CNS penetration, highlighting the potential of these effective triazene based-hybrids for enhanced anticancer chemotherapy.

1. Introduction

Brain tumors have surpassed leukemia as the leading cause in cancer deaths among children and their incidence is relatively high in the adult population, with gliomas accounting for 82% of all malignant brain tumors [1,2]. Glioblastoma multiforme (GBM), the most lethal type of glioma, presents an average patient's survival time of only 14 months. Current treatment for GBM patients includes surgical tumor resection followed by radiotherapy with concomitant and adjuvant chemotherapy based on temozolomide (TMZ, Fig. 1) [3]. TMZ is a triazene that has shown promising antitumor activity not only in brain tumors, but also in a variety of solid tumors, including malignant melanoma. TMZ can be taken orally and, due to its small size and lipophilic features, it is able to cross the blood-brain barrier [4]. Once in the central nervous system, TMZ undergoes hydrolytic ring opening at physiological pH to a monomethyltriazene intermediate that spontaneously decomposes to release the highly reactive methyldiazonium cation, responsible for DNA alkylation [5]. However, the widespreading nature of glioma cells disrupts TMZ efficacy, resulting in high recurrence of glioblastoma. Proliferation and cell migration, along with every DNA repair system activated throughout the complex key signaling pathways of GBM, remain some of the demanding challenges for successful therapy [6]. The anticonvulsant valproic acid (VPA, Fig. 1) was recently identified as a short chain fatty acid (SCFA) histone deacetylase (HDAC) inhibitor that prevents cell proliferation in GBM brain cancer and modulates several transcription factors [7]. Phase II clinical trials showed improvement in the outcome of patients with GBM when VPA was combined with the standard treatment (TMZ plus radiotherapy); a median overall survival of 29.6 months was obtained with this combination, compared to 14.6 months with the standard protocol [3,8]. Further investigations also revealed that VPA induces chromatin loosening, thus increasing TMZ accessibility to DNA and leading to higher methylation levels [9].

We have recently reported the activity of a triazene-VPA hybrid compound, **1a** (HYBCOM, Fig. 1), against glioma GL261 cells [10]. The loss of cell viability induced by **1a** was preferentially sensed by glioma cells and did not significantly affect normal astrocytes. In addition to reduced cell viability, there was also a higher decrease in cell proliferation when compared to TMZ. Remarkably, compared

Abbreviations: BBB, blood-brain barrier; CDI, 1,1′-carbonyldiimidazole; CNS MPO, central nervous system multiparameter optimization; DCC, N,N′-dicyclohexylcarbodiimide; ESI-HRMS, High resolution electrospray ionization mass spectrometry; GBM, glioblastoma multiforme; HDAC, histone deacetylase; HOBt, hydroxybenzotriazole; MMT, monomethyltriazene; PBS, phosphate buffered saline; SCFA, short chain fatty acid; TMZ, temozolomide; VPA, valproic acid.

* Corresponding author.
E-mail address: mjprocha@ff.ulisboa.pt (M.J. Perry).

https://doi.org/10.1016/j.ejmech.2019.03.048
0223-5234/

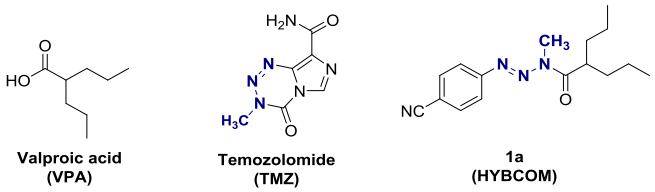

Fig. 1. The chemical structures of valproic acid (VPA), temozolomide (TMZ), and HYBCOM.

to TMZ, **1a** enhanced the susceptibility of GL261 cells to shape alteration, from a polar to a non-polar morphology, which may be related to a decline in cell migratory ability. Moreover, in contrast to TMZ, cells exposed to **1a** maintained drug resistance levels close to control conditions. To better understand the structural requirements of *N*-acyltriazenes to target glioma cells, we herein disclose the structure-activity relationship (SAR) and mechanistic studies of a series of *N*-acyltriazenes and their anti-glioma activity. These hybrid compounds contained differently substituted triazene moieties and HDAC inhibitor-related short chain fatty acids, including valproic and butyric acids, and displayed a broad range of stereoelectronic and lipophilicity properties (Scheme 1, **1a-k**). Biological assays towards the GL261 glioma cell line revealed analogue **1d** as the most potent in the series, with selective targeting of GL261 glioma cells *versus* SH-SY5Y neuronal cells, and showing high induction of cell morphological alterations that led to cell migration impairment.

2. Results and discussion

2.1. Chemistry

Compounds **1a**–**k** were synthesized as depicted in Scheme 1 adapting a previously reported procedure [10]. Diazotization of commercially available anilines **2**, followed by reaction with formaldehyde and methylamine, afforded the corresponding hydroxymethyltriazenes **3** [11], which were then converted to the respective monomethyltriazenes (MMT) **4** in the presence of a three-fold excess of methylamine [12]. Coupling of MMTs **4** with the appropriate carboxylic acid using CDI or DCC, combined with 1-hydroxybenzotriazole (HOBt), afforded the desired hybrid compounds **1a-k** in moderate to good yields.

To predict the BBB penetrance of the novel triazenes, Pfizer's CNS multiparameter optimization (MPO) score was determined [13]. CNS MPO scores span from 0 to 6.0 based on the optimal ranges of several physicochemical properties, and improved BBB penetration is usually associated to MPO values $\geq$ 4. The MPO values for **1a**-**k** range from 4.0 to 5.5, suggesting that these compounds may achieve effective drug concentrations in the brain (Table S1).

2.2. Biological evaluation

2.2.1. Cytotoxicity and cell death in GL261 and SH-SY5Y cell lines

We first explored the cytotoxic effects of *N*-acyltriazenes **1a-k** in the GL261 mouse glioma cell line, at concentrations between 0.1 and 100 μM, using TMZ for comparative purposes (Figure S1). The resulting IC_{50} values are presented in Table 1 and reveal that compounds **1c-g** were more potent than both TMZ and **1a** in inducing cell cytotoxicity. Remarkably, valproate derivatives **1d** and **1e** presented IC_{50} values of 12 and 7 μM, respectively, *i.e.,* at least 10-fold more potent than the lead compound **1a**. Triazene derivatives with shorter acyl moieties **1i-k** did not induce appreciable cytotoxicity in the range of concentrations tested. Overall, from all the screened compounds, we selected valproate derivates **1d** ($R^1 = CONH_2$) and **1e** ($R^1 = CO_2Me$) at 10 μM for the subsequent evaluation.

We previously reported that the lead compound **1a**, although affecting cell viability, did not produce significant alteration of necrosis in GL261 cells [10]. Therefore, we decided to evaluate whether **1d** and **1e** showed a similar pattern, by determining the percentage of viable, early apoptotic and late-apoptotic/necrotic cells by flow cytometry. As indicated in Fig. 2, hybrid compounds **1a**, **1d** and **1e** decreased cell viability (Fig. 2A) and increased early apoptosis (Fig. 2B). However, only **1d** was able to induce late apoptosis/necrosis in GL261 cells (Fig. 2C), in addition to being the one causing the highest loss of cell viability among the tested compounds (Fig. 2A).

Then, we evaluated if these compounds showed increased cell death specificity toward glioma cells compared to other cell types, like the differentiated SH-SY5Y neuronal cell line. Despite their neuroblastoma cell origin, differentiated SH-SY5Y cells possess a mature phenotype, with the presence of neuronal markers, such as

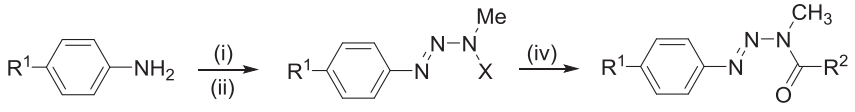

2a-h

2a-4a: R^1 = CN
2b-4b: R^1 = COOEt
2c-4c: R^1 = COMe
2d-4d: R^1 = $CONH_2$
2e-4e: R^1 = COOMe
2f-4f: R^1 = Cl
2g-4g: R^1 = Br
2h-4h: R^1 = CH_3

3a-h
X = CH_2OH

4a-h
X = H

1a-k

1a: R^1 = CN; R^2 = $CH(CH_2CH_2CH_3)_2$
1b: R^1 = COOEt; R^2 = $CH(CH_2CH_2CH_3)_2$
1c: R^1 = COMe; R^2 = $CH(CH_2CH_2CH_3)_2$
1d: R^1 = $CONH_2$; R^2 = $CH(CH_2CH_2CH_3)_2$
1e: R^1 = COOMe; R^2 = $CH(CH_2CH_2CH_3)_2$
1f: R^1 = Cl; R^2 = $CH(CH_2CH_2CH_3)_2$
1g: R^1 = Br; R^2 = $CH(CH_2CH_2CH_3)_2$
1h: R^1 = CH_3; R^2 = $CH(CH_2CH_2CH_3)_2$
1i: R^1= CN; R^2 = $CH_2CH_2CH_3$
1j: R^1 = CN; R^2 = $CH(CH_3)_2$
1k: R^1 = CN; R^2 = $CH(CH_2CH_3)_2$

Scheme 1. Synthetic route for the hybrid compounds **1a-k**. (i) $NaNO_2$, conc. HCl, H_2O, 0–5 °C; (ii) HCHO/$MeNH_2$, rt (iii) $MeNH_2$, H_2O, rt; (iv) R^2COOH, **4a-h**, coupling reagent/HOBt, NaH, THF.

Table 1
IC_{50} values against glioma GL261 cells, half-lives ($t_{½}$) in PBS buffer (10 mM, pH = 7.4) and human plasma (80% v/v) for the hydrolysis to the corresponding monomethyltriazenes and anilines, and CNS MPO scores for **1a-k** and TMZ.

Compd.	CNS MPO [13]	IC_{50} (μM)[a]	Half-life $t_{1/2}$ (h)	
			pH 7.4 phosphate buffer	80% (v/v) human plasma
1a	4.2	>100[b]	>40	>40
1b	4.0	>100[b]	34.1 ± 0.4	>40
1c	4.2	47.0 ± 3.65	>40	>40
1d	4.6	11.9 ± 5.78	>40	>40
1e	4.1	6.7 ± 1.48	31.4 ± 0.3	>40
1f	4.0	58.4 ± 6.65	27.3 ± 0.3	>40
1g	4.0	80.6 ± 8.15	30.4 ± 0.1	>40
1h	4.0	>100[b]	31.3 ± 0.5	>40
1i	5.4	>100[b]	>40	15.2 ± 0.7
1j	5.5	>100[b]	>40	13.9 ± 1.1
1k	4.8	>100[b]	>40	>40
TMZ	4.9 [14]	>100[b]	–	–

[a] Four independent experiments.
[b] 100 μM was the highest concentration tested.

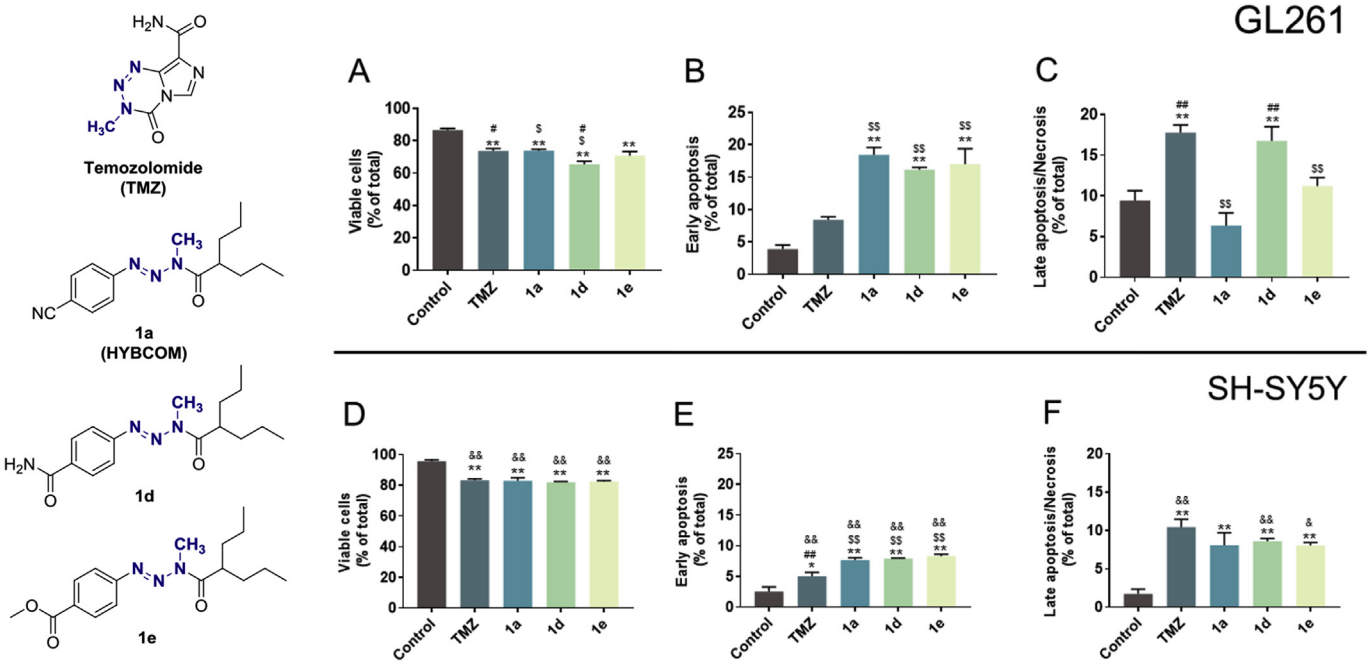

Fig. 2. Changes in glioma and neuronal cell viability by temozolomide (TMZ) and hybrid compounds **1a**, **1d** and **1e**. Mouse GL261 glioma (A–C) and human SH-SY5Y neuronal (D–F) cell lines were treated with TMZ or **1a**, **1d** and **1e** hybrid compounds at a concentration of 10 μM during 48 h. The percentages of viable cells (A,D) and cells in early- (B,E) and late-apoptosis/necrosis (C,F) were determined by flow cytometry with phycoerythrin-conjugated annexin V (annexinV-PE) and 7-amino-actinomycin D (7-AAD). The three populations were distinguished as follows: viable cells (annexin V-PE and 7-AAD negative), early apoptotic cells (annexinV-PE positive and 7-AAD negative), and cells in late stages of apoptosis or dead cells (annexinV-PE and 7-AAD positive). All results are means ± SEM from three independent experiments performed in duplicate. Comparisons were conducted by one-way ANOVA followed by multiple comparisons Bonferroni post hoc correction. **p < 0.01 vs. non-treated cells (control); $p < 0.05, $$p < 0.01 vs. cells treated with TMZ; #p < 0.05, ##p < 0.01 vs. cells treated with **1a**; &p < 0.05, &&p < 0.01 vs. GL261 cells treated with the same compound.

βIII-tubulin, microtubule-associated protein-2 (MAP2), synaptophysin, NeuN, synaptic associated protein-97 (SAP-97) and growth-associated protein 43 (GAP43) [15]. As indicated in Fig. 2D, we verified that hybrid compounds **1a**, **1d** and **1e**, as well as TMZ, reduced neuronal cell viability but with lower efficiency than in glioma cells (Fig. 2A). Moreover, the induced levels of early apoptosis and late necrosis on neuronal cells (Fig. 2E–F) were roughly only one half of those produced in glioma cells (Fig. 2B–C), revealing that the tested compounds have cell type-specific toxicity.

2.2.2. *Modulation of invasive GL261 cell properties*

Next, we evaluated if the *N*-acyltriazenes were able to modulate cytoskeleton organization in GL261 cells, *e.g.* by promoting a switch from a polar to a non-polar morphology and a decline in their migratory ability properties as observed for **1a** [10]. With the exception of TMZ, all test compounds were able to increase cell circularity, decreasing their aspect ratio (width/height) (Fig. 3), which is compatible with a non-polar morphology of the glioma cells [16]. Importantly, **1d** and **1e** were more effective than **1a** in causing such morphological alteration.

The observed morphological changes in GL261 cells by the hybrid compound **1a** were previously shown to be associated with reduced cell migration ability [10]. As indicated in Fig. 4, the same effect was observed for all the compounds tested in the present study. Interestingly, **1d** was also the most efficient in causing

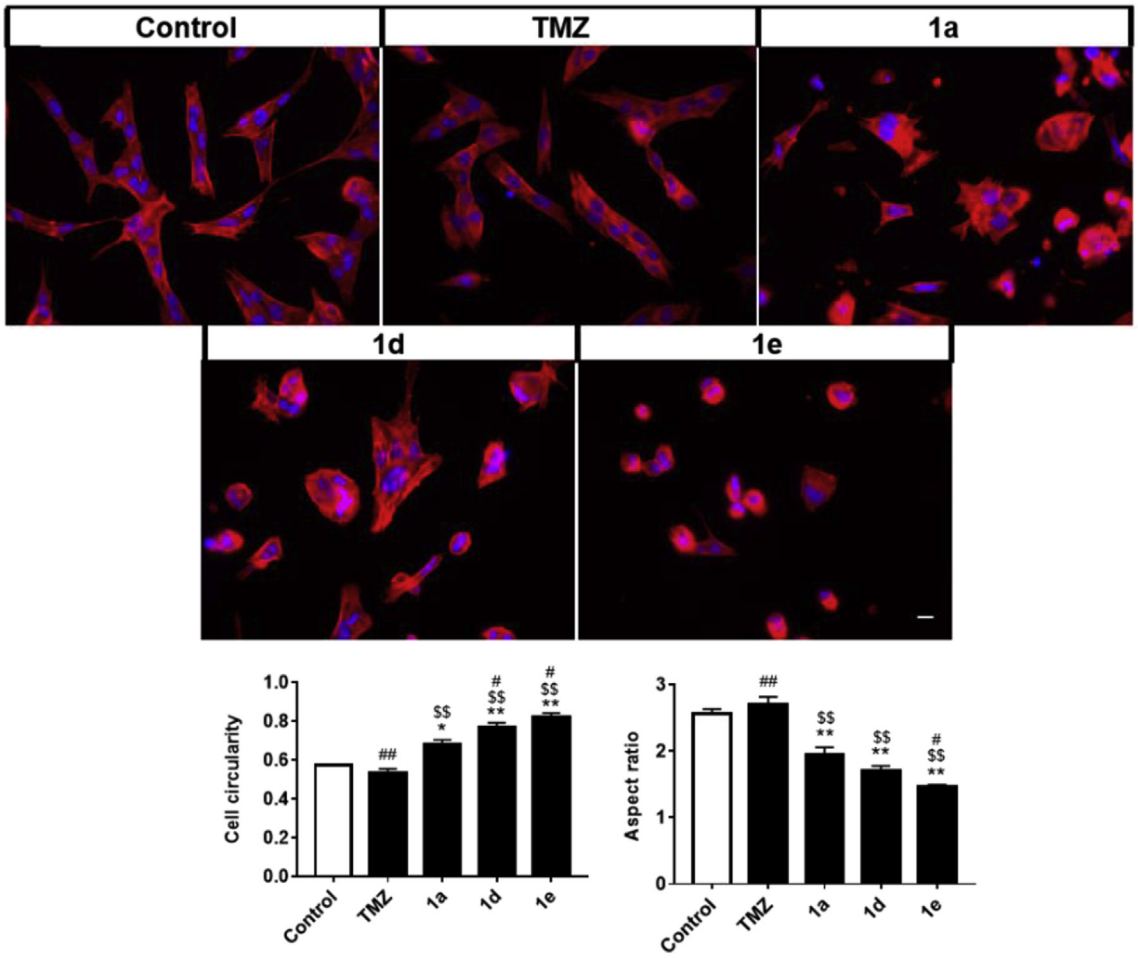

Fig. 3. Changes in glioma cell morphology by temozolomide (TMZ) and hybrid compounds **1a**, **1d** and **1e**. Mouse GL261 glioma cells were treated with TMZ or the hybrid compounds at a concentration of 10 μM during 48 h. Representative results of one experiment are shown. Cell circularity and aspect ratio were quantified by manual tracings using ImageJ® software. Results are expressed as mean ± SEM from three independent experiments. *p < 0.05, **p < 0.01 *vs.* non-treated cells (control); $$p < 0.01 *vs.* cells treated with TMZ; #p < 0.05, ##p < 0.01 *vs.* cells treated with **1a**. The scale bar represents 20 μm.

reduction of glioma cell migration, thus showing to be highly effective in protection against cell invasiveness. Taken together, our data indicate **1d** and **1e** as the most promising compounds in altering glioma cell morphology and decreasing cell migration ability, properties that are implicated in glioblastoma cell invasion and malignancy [17]. Moreover, **1d** also demonstrated an elevated necrotic potential toward glioma cells.

2.3. HDAC inhibition assays

Since valproic acid is a known, albeit weak, HDAC inhibitor [18], we decided to evaluate if the ability displayed by *N*-acyltriazenes to induce a non-polar morphology and decrease cell migration in GL261 cells could be associated to HDAC inhibition. Compounds **1a-k** were studied using commercially available HDAC fluorometric activity assay (Table S2). All compounds were very weak HDAC inhibitors, with less than 10% inhibition of enzyme activity at 6.25 μM. These results are in line with the weak HDAC inhibitory activity reported for linear and branched short-chain carboxylic acids, including valproic and butyric acids [19]. Although valproate **1b** and butyrate **1i** derivates were able to reduce HDAC activity by ca. 50% at 100 μM, no obvious correlation emerged between enzyme inhibitory potency and anti-glioma activity.

2.4. DNA alkylation assays

In our previous study, the intra- and extracellular **1a** concentrations were measured by liquid chromatography-tandem mass spectrometry (LC-MS/MS) and we observed that this compound was effectively incorporated into the cells, remaining without degradation until 72 h [10]. Nevertheless, *N*-Acyltriazenes are known to undergo deacetylation to the corresponding monomethyltriazenes with subsequent generation of the methyldiazonium cation [20]. In order to assess the possibility of *N*-acyltriazenes exerting their anti-glioma activity *via* DNA alkylation, we incubated compound **1a** with a selected single stranded oligonucleotide. DNA sequences with runs of purines have been reported to be more reactive towards alkylation by triazene derivatives [21,22]. In general, the site of greatest alkylation occurs at runs of two or three contiguous guanines, with the inner guanines showing higher alkylation than isolated guanines. Supported by these prior observations, the deoxyoligonucleotide base sequence chosen in this study was designed as 5' – GGG AGA – 3'. Incubation with the single-stranded oligonucleotide was assayed at 1:3, 1:10, 1:100 and 1:250 M ratios of oligonucleotide to either compound **1a** or the corresponding monomethyltriazene **4a**. No modification was observed by high resolution mass spectrometry when the single-stranded oligonucleotide was incubated for 7-days

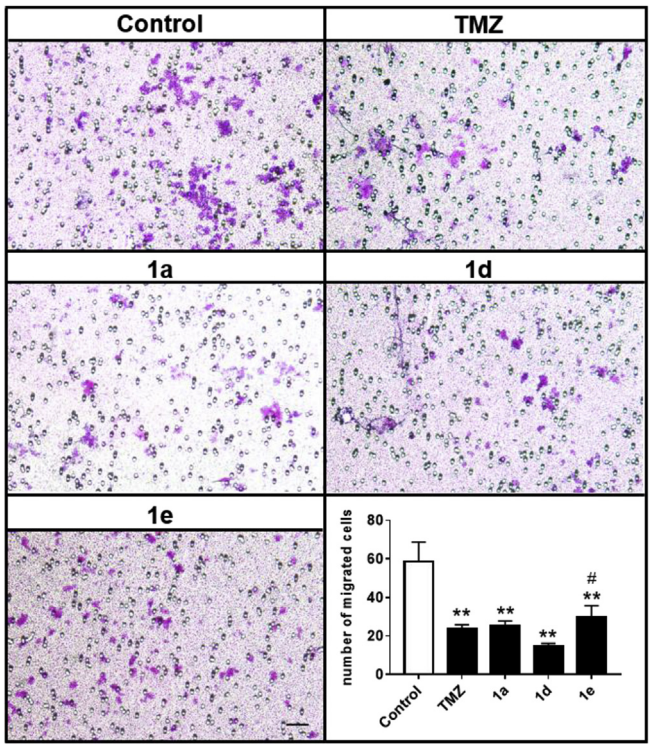

Fig. 4. Changes in glioma cell migration ability by temozolomide (TMZ) and hybrid compounds **1a**, **1d** and **1e**. Mouse GL261 glioma cells were treated with TMZ or the hybrid compounds at a concentration of 10 μM during 48 h. Migration was assessed using a Boyden Chamber. Non-treated (control) and treated cells were allowed to migrate for 6 h. Representative results of one experiment are shown. The total number of cells per well was counted and the results represent the average of migrated cells counted in each well. Results are expressed as mean ± SEM from four independent experiments. $^{**}p < 0.01$ *vs.* non-treated cells (control); $\#p < 0.05$ *vs.* cells treated with **1a**. The scale bar represents 20 μm.

with **1a** in any of the tested concentrations. In contrast, the monomethyltriazene **4a** was able to modify the oligodeoxynucleotide at a 1:250 M ratio, after 1 h incubation. The identification of two group of peaks at *m/z* 946.1857 and 630.4559, assigned to a doubly- and a triply-charged methylated oligonucleotide species, respectively, indicates the formation of a monomethylated adduct (O^6-MeG). However, the data could not unequivocally establish which guanine was methylated. The ESI(−)/HRMS mass spectra, together with the accurate mass measurements for the identified species, are presented in Fig. 5. These results clearly indicate that compound **1a** does not alkylate the oligonucleotide, while its monomethyltriazene **4a** counterpart was able to promote methylation in the O^6 position of guanine base(s) *in vitro*.

2.5. Stability evaluation

The lack of oligonucleotide methylation observed with **1a** prompted us to study the chemical stability of compounds **1a-k** in pH 7.4 buffer, at 37 °C. Data depicted in Table 1 reveal that compounds **1a-k** hydrolyze very slowly to the corresponding monomethyltriazenes and anilines at physiological pH, with half-live values higher than 25 h, *i.e.*, the tested compounds are significantly more stable than TMZ and its derivatives (*e.g.* $t_{1/2} > 40$ h for **1d** when compared to 2 h for TMZ [14] in PBS). Overall, the rate of hydrolysis at pH 7.4 was not significantly affected by the nature of substituents in the aryltriazene moiety or the α-branching at the acyl moiety. These results contrast with those reported for *N*-acylamino acid derivatives of triazenes, where electron-attracting substituents in the aryltriazene moiety increased the rate of hydrolysis, while α-branching at the acyl moiety had a detrimental effect on reactivity at pH 7.4 [20,23]. This discrepancy might be ascribed to different contributions of the hydroxide and buffer-catalyzed pathways to the hydrolysis of compounds **1** and their *N*-acylamino acid counterparts. Worth of note, compound **1a** also showed to be stable when incubated with *N*-acetylcysteine and glutathione (Figure S2). Remarkably, valproate derivatives of triazenes, **1a-h**, were stable in human plasma, showing no measurable decomposition over 2 days. In contrast, the less hindered *n*-propyl (butyrate), **1i**, and *i*-propyl, **1j**, derivatives were hydrolyzed to the corresponding monomethyltriazene and aniline with half-lives of 15 and 14 h, respectively. Introducing an α-ethyl substituent in the *n*-propyl side chain, *i.e.* **1k**, led to a dramatic decrease in the reactivity towards amidases. For the less hindered triazene derivatives **1i** and **1j** it was possible to monitor the hydrolysis conversion into the corresponding products (Figure S3), suggesting that these compounds have the potential to release the DNA-alkylating methyldiazonium ion in the blood circulation. Indeed, serum albumin has been reported to increase the half-lives of the parent monomethyltriazenes [24]. The high stability of triazenes **1a-h** and **1k** in human plasma may also result from protein binding, as plasma protein-bound drugs are partially protected from hydrolysis.

Further studies must be performed to clarify the impact on the plasma pseudo-first order hydrolysis rate constants. As previously reported, decomposition of monomethyltriazenes is catalyzed by divalent metal ions [25]. Blood concentrations of Cu^{2+} and Zn^{2+} are 15 μM and 100 μM, respectively [26], and thus these ions could be an important factor in determining the stability of *N*-acyltriazenes. To gain further insight into the effect of metals on the reactivity of *N*-acyltriazenes, we monitored by UV–Vis spectroscopy the reaction of compounds **1b** and **1i** and their monomethyltriazene counterparts **4b** and **4a**, respectively, in methanolic solutions of Cu^{2+} and Zn^{2+} (Figures S4 and S5). Compounds **1b** and **1i** did not decompose to the corresponding anilines **2** in the presence of any of the metals (Figure S4). In contrast, monomethyltriazenes **4a** and **4b** were rapidly converted to the corresponding anilines in the presence of Cu^{2+} (Figure S5, A and B). Zinc-catalyzed decomposition was also observed for **4a** and **4b** but at a slower rate when compared with the Cu^{2+}-catalyzed reaction (Figure S5, C and D), in line with the reported higher catalytic efficiency of Cu^{2+} on the decomposition of monomethyltriazenes [25].

3. Conclusions

The studies herein presented led to the identification of novel hybrid compounds with a remarkable increase in potency toward glioma GL261 cells compared to the lead compound **1a**. Cytotoxicity assays highlighted **1d** and **1e** as having the highest anti-tumor efficacy, including high potency (IC_{50} 11.9 μM and 6.7 μM, respectively) together with an effective decrease of invasive cell properties. CNS MPO scores suggest that **1d** and **1e** are BBB-penetrant. In contrast to temozolomide, which undergoes hydrolysis to release the alkylating metabolite monomethyltriazene, the valproate derivatives studied **1a-h** showed enhanced chemical and metabolic stability combined with a low potential to alkylate DNA. Triazenes **1** revealed to be weak HDAC inhibitors, suggesting that this class of enzymes is not the main target for these compounds. Overall, these results validate valproate-triazene hybrid compounds as a new class of anti-glioma agents with clear chemotherapeutic advantages over temozolomide, and thus with potential to be used in the chemotherapy of glioblastoma.

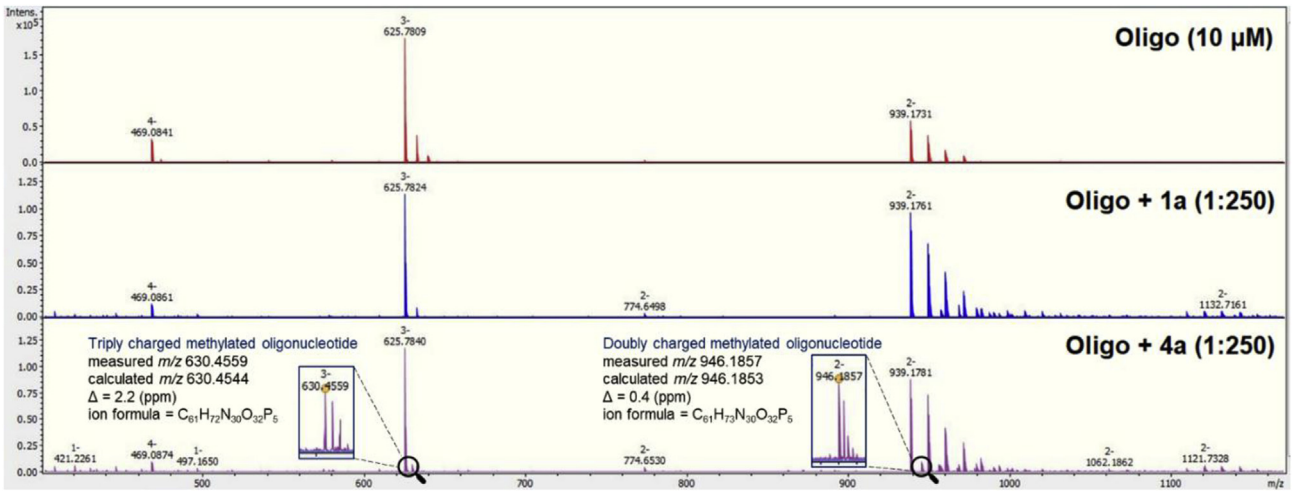

Fig. 5. Comparison of the ESI(−)/HRMS profiles of **1a** (HYBCOM) and **4a** incubated with 5′ − GGG AGA − 3′ in ammonium bicarbonate buffer (10 mM, pH 8.3) at 37 °C.

4. Experimental

4.1. General information

All reagents and solvents were purchased from commercial suppliers. All solvents were purified by standard techniques. Reactions were monitored by thin-layer chromatography using silica-gel aluminum sheets (Merck Kieselgel 60 F_{254}). Column chromatography was performed using Merck silica gel 60 (230–400 mesh ASTM). Melting points were determined using a Kofler camera Bock-Monoscop "M" and are uncorrected. ^{1}H and ^{13}C NMR spectra were recorded in $CDCl_3$ solutions using a Bruker Ultra-Shield 300 MHz spectrometer; chemical shifts (δ) are reported in parts per million (ppm) relative to tetramethylsilane (TMS) as internal standard and coupling constants (J) are expressed in hertz (Hz). High-performance liquid chromatography was performed in an Elite LaChrom (VWR Hitachi) system comprised of an L-2130 pump, an L-2400 UV detector and a Rheodyne® manual sample injector, including a 20 μL sample loop. Chromatographic separation was achieved on a Lichrospher® 100 RP-18 (5 μm) using an isocratic solvent elution at a flow rate of 1.0 mL min^{-1}. Water/acetonitrile (35:65) was chosen for compounds **1a** and **1i-k**, while water/acetonitrile (20:80) was preferred for compounds **1b-h**. Purity of compounds as determined by HPLC, was higher than 95%. According to the λ_{max} of compounds, the UV detector was set at 300 nm. Low resolution mass spectra were recorded using a Micromass Quattro Micro API spectrometer. High-resolution mass spectra (HRMS) were acquired on a QqTOF Impact II (Bruker Daltoniks) mass spectrometer equipped with an electrospray source operating in positive and negative mode, interfaced in line with a Dionex UltiMate® 3000 RSLCnano (Thermo Fisher Scientific Inc.). Aliquots (10 μL) of the samples were analyzed by flow injection analysis (FIA) using an isocratic gradient 50 A:50 B of 0.1% formic acid in water (A) and 0.1% of formic acid in acetonitrile (B), at a flow rate of 10 μL min^{-1}, over 15 min. The mass spectrometer parameters were set as follows: capillary voltage: +4.5 and −2,5 kV (positive and negative mode, respectively); end plate offset: 500 V; nebulizer: 40 psi; dry gas: 4.0 L min^{-1}; dry heather: 200 °C. Prior to analysis, the TOF analyzer was calibrated by infusion of ESI Low Concentration Tune Mix (Agilent Technologies) at a 15 μL min^{-1} flow rate. Recalibration of acquired data was performed *via* lock mass internal calibration (1221.9906) located within the source. Acquisition was performed in full scan mode over a mass range of 100–2000 m/z with an acquisition rate of 1 Hz. Data was processed using Data Analysis 4.2 software.

Compounds **3** and **4** were synthesized by previously published methods [11,12]. 5′–GGG AGA–3′ was purchased from STAB VIDA (Lisbon, Portugal) and used without further purification. The oligonucleotide was dissolved in water and 100 μM stock solutions were prepared and kept at −18 °C until required.

4.2. General procedure for the synthesis of compounds 1

Method A: CDI-mediated amide coupling (**1b-d**, **1f-g** and **1i-k**). To a solution of the appropriate acid (0.55 mmol) in 2 mL of THF, was added anhydrous HOBt (81 mg, 0.6 mmol). The reaction mixture was stirred at room temperature for 15 min. Subsequently, CDI (97 mg, 0.6 mmol) was added in one portion, turning the solution from milky white to colorless, with CO_2 release. The solution was stirred for 45 min, under nitrogen atmosphere. Triethylamine (166 μL, 1.2 mmol) and monomethyltriazene (0.6 mmol), previously activated with NaH (60% dispersion in mineral oil, 24 mg, 0.6 mmol) in methylene chloride (5 mL) were added and the reaction mixture was stirred for 48 h. When complete, the reaction mixture was quenched with 1 mL of 1 M HCl and stirred vigorously for 10 min, and the aqueous layer was extracted with methylene chloride (2 × 2 mL). The combined organic layers were washed sequentially with 1 M HCl (2 mL), deionized water (2 mL), and a 1:1 aqueous mixture of brine and saturated $NaHCO_3$ (4 mL). The organic layer was dried with Na_2SO_4 and the solvent was removed under reduced pressure to give the crude product. All compounds were purified by column chromatography and obtained with purity >95%.

Method B: DCC-mediated amide coupling (**1e** and **1h**). Similar to Method A but using DCC as coupling agent.

4.2.1. 1-(4-cyanophenyl)-3-methyl-3-[2-(propyl)pentanoyl] triazene (*1a*)

Synthesis and purification were followed according to previous reported procedures [10].

4.2.2. 1-(4-ethoxycarbonylphenyl)-3-methyl-3-[2-(propyl) pentanoyl]triazene (*1b*)

Method A was followed using 1-(4-ethoxycarbonylphenyl)-3-methyltriazene and sodium valproate. The final mixture was purified by column chromatography (methylene chloride) to yield the

product as a brown oil (43.3%). ^{1}H NMR (300 MHz, $CDCl_3$) δ 8.13 (2H, d, $J = 8.8$ Hz), 7.63 (2H, d, $J = 8.8$ Hz), 4.39 (2H, q, $J = 7.1$ Hz), 3.69–3.75 (1H, m), 3.47 (3H, s), 1.70–1.83 (2H, m), 1.46–1.55 (2H, m), 1.41 (3H, t, $J = 7.1$ Hz), 1.24–1.33 (4H, m), 0.88 (6H, t, $J = 7.3$ Hz); ^{13}C NMR (75 MHz, $CDCl_3$) δ 179.42, 166.19, 152.28, 130.87, 130.52, 121.97, 61.30, 41.96, 35.16, 28.11, 20.87, 14.47, 14.28; HR-ESI(+)/MS: *m/z* calcd for $C_{18}H_{28}N_3O_3$ $[M + H]^+$: 334.2125; found 334.2129.

4.2.3. 1-(4-acetylphenyl)-3-methyl-3-[2-(propyl)pentanoyl] triazene (**1c**)

Method A was followed using 1-(4-acetylphenyl)-3-methyltriazene and sodium valproate. The final mixture was purified by column chromatography (methylene chloride) to yield the product as an orange oil (37.8%); ^{1}H NMR (300 MHz, $CDCl_3$) δ 8.05 (2H, d, $J = 8.8$ Hz), 7.66 (2H, d, $J = 8.8$ Hz), 3.67–3.76 (1H, m), 3.47 (3H, s), 2.63 (3H, s), 1.70–1.83 (2H, m), 1.47–1.58 (2H, m), 1.23–1.36 (4H, m), 0.88 (6H, t, $J = 7.3$ Hz); ^{13}C NMR (75 MHz, $CDCl_3$) δ 197.37, 179.38, 152.35, 136.93, 129.71, 122.21, 41.95, 35.15, 28.15, 26.85, 20.86, 14.28; HR-ESI(+)/MS: *m/z* calcd for $C_{17}H_{26}N_3O_2$ $[M + H]^+$: 304.2020; found 304.2025.

4.2.4. 1-(4-carbamoylphenyl)-3-methyl-3-[2-(propyl)pentanoyl] triazene (**1d**)

Method A was followed using 1-(4-carbamoylphenyl)-3-methyltriazene and sodium valproate. The final mixture was purified by column chromatography (ethyl acetate) to yield the product as a yellow solid (56.2%); m.p. 105–107 °C; ^{1}H NMR (300 MHz, $CDCl_3$) δ 7.92 (2H, d, $J = 8.7$ Hz), 7.64 (2H, d, $J = 8.7$ Hz), 6.36 (2H, bs), 3.68–3.74 (1H, m), 3.46 (3H, s), 1.69–1.81 (2H, m), 1.46–1.57 (2H, m), 1.22–1.34 (4H, m), 0.87 (6H, t, $J = 7.3$ Hz); ^{13}C NMR (75 MHz, $CDCl_3$) δ 179.41, 169.03, 151.63, 133.36, 128.70, 122.23, 41.92, 35.13, 28.08, 20.83, 14.26; HR-ESI(+)/MS: *m/z* calcd for $C_{16}H_{25}N_4O_2$ $[M + H]^+$: 305.1972; found 305.1980.

4.2.5. 1-(4-methoxycarbonylphenyl)-3-methyl-3-[2-(propyl) pentanoyl]triazene (**1e**)

Method B was followed using 1-(4-methoxycarbonylphenyl)-3-methyltriazene and sodium valproate. The final mixture was purified by column chromatography (methylene chloride) to yield the product as an orange oil (33.0%); ^{1}H NMR (300 MHz, $CDCl_3$) δ 8.13 (2H, d, $J = 8.8$ Hz), 7.64 (2H, $J = 8.8$ Hz), 3.94 (3H, s), 3.69–3.75 (1H, m), 3.47 (3H, s), 1.71–1.83 (2H, m), 1.47–1.58 (2H, m), 1.23–1.36 (4H, m), 0.88 (6H, t, $J = 7.3$ Hz); ^{13}C NMR (75 MHz, $CDCl_3$) δ 179.37, 166.63, 152.33, 130.90, 130.14, 122.00, 52.38, 41.95, 35.14, 28.09, 20.84, 14.26; HR-ESI(+)/MS: *m/z* calcd for $C_{17}H_{26}N_3O_3$ $[M + H]^+$: 320.1969; found 320.1974.

4.2.6. 1-(4-chlorophenyl)-3-methyl-3-[2-(propyl)pentanoyl] triazene (**1f**)

Method A was followed using 1-(4-chlorophenyl)-3-methyltriazene and sodium valproate. The final mixture was purified by column chromatography (hexane: ethyl acetate - 4:1) to yield the product as a brown oil (87.2%); ^{1}H NMR (300 MHz, $CDCl_3$) δ 7.54 (2H, $J = 8.9$ Hz), 7.41 (2H, d, $J = 8.9$ Hz), 3.66–3.75 (1H, m), 3.44 (3H, s), 1.69–1.82 (2H, m), 1.45–1.57 (2H, m), 1.22–1.34 (4H, m), 0.87 (6H, t, $J = 7.3$ Hz); ^{13}C NMR (75 MHz, $CDCl_3$) δ 179.29, 147.58, 134.63, 129.51, 123.35, 41.89, 35.18, 27.94, 20.86, 14.29; HR-ESI(+)/MS: *m/z* calcd for $C_{15}H_{22}ClN_3O$ $[M + Na]^+$: 318.1344; found 318.1350/320.1324.

4.2.7. 1-(4-bromophenyl)-3-methyl-[2-(propyl)pentanoyl]triazene (**1g**)

Method A was followed using 1-(4-bromophenyl)-3-methyltriazene and sodium valproate. The final mixture was purified by column chromatography (hexane: ethyl acetate - 4:1) to yield the product as a brown oil (46.1%). ^{1}H NMR (300 MHz, $CDCl_3$) δ 7.57 (2H, d, $J = 8.8$ Hz), 7.47 (2H, d, $J = 8.8$ Hz), 3.65–3.74 (1H, m), 3.44 (3H, s), 1.69–1.82 (2H, m), 1.45–1.57 (2H, m), 1.22–1.35 (4H, m), 0.87 (6H, t, $J = 7.3$ Hz); ^{13}C NMR (75 MHz, $CDCl_3$) δ 179.26, 148.00, 132.47, 123.64, 122.77, 41.88, 35.16, 27.95, 20.84, 14.28; HR-ESI(+)/MS: *m/z* calcd for $C_{15}H_{22}BrN_3O$ $[M + Na]^+$: 362.0836; found 362.0848/364.0824.

4.2.8. 3-Methyl-3-[2-(propyl)pentanoyl]-1-(4-tolyl)triazene (**1h**)

Method B was followed using 3-methyl-1-(*p*-tolyl)triazene and sodium valproate. The final mixture was purified by column chromatography (hexane: ethyl acetate - 4:1) to yield the product as a brown oil (yield 27.5%); ^{1}H NMR (300 MHz, $CDCl_3$) δ 7.51 (2H, d, $J = 8.3$ Hz), 7.25 (2H, d, $J = 7.9$ Hz), 3.68–3.79 (1H, m), 3.44 (3H, s), 2.40 (3H, s) 1.71–1.83 (2H, m), 1.46–1.57 (2H, m), 1.24–1.36 (4H, m), 0.88 (6H, t, $J = 7.2$ Hz); ^{13}C NMR (75 MHz, $CDCl_3$) δ 179.36, 146.91, 139.19, 129.93, 122.03, 41.82, 35.22, 27.70, 21.38, 20.86, 14.29; HR-ESI(+)/MS: *m/z* calcd for $C_{16}H_{25}N_3O$ $[M + Na]^+$: 298.1890; found 298.1895.

4.2.9. 3-Butyryl-1-(4-cyanophenyl)-3-methyltriazene (**1i**)

Method A was followed using 1-(4-cyanophenyl)-3-methyltriazene and butyric acid. The final mixture was purified by column chromatography (methylene chloride) to yield the product as a yellow solid (yield 22.9%); m.p. 55–57 °C; ^{1}H NMR (300 MHz, $CDCl_3$) δ 7.74 (2H, d, $J = 8.8$ Hz), 7.66 (2H, d, $J = 8.8$ Hz), 3.44 (3H, s), 2.91 (2H, t, $J = 7.4$ Hz), 1.72–1.84 (2H, m), 1.02 (3H, t, $J = 7.4$ Hz); ^{13}C NMR (75 MHz, $CDCl_3$) δ 175.75, 151.97, 133.45, 122.78, 118.68, 112.10, 36.21, 28.19, 18.51, 14.04; HR-ESI(+)/MS: *m/z* calcd for $C_{12}H_{14}N_4O$ $[M + Na]^+$: 253.1060; found 253.1059.

4.2.10. 1-(4-cyanophenyl)-3-isobutyryl-3-methyltriazene (**1j**)

Method A was followed using 1-(4-cyanophenyl)-3-methyltriazene and isobutyric acid. The final mixture was purified by column chromatography (methylene chloride) to yield the product as an orange solid (yield 32.4%); m.p. 110–112 °C; ^{1}H NMR (300 MHz, $CDCl_3$) δ 7.74 (2H, d, $J = 8.8$ Hz), 7.67 (2H, d, $J = 8.8$ Hz), 3.66 (1H, hept, $J = 6.9$ Hz), 3.45 (3H, s), 1.26 (6H, d, $J = 6.9$ Hz); ^{13}C NMR (75 MHz, $CDCl_3$) δ 179.68, 152.04, 133.48, 122.78, 118.69, 112.12, 32.10, 28.41, 19.41; HR-ESI(+)/MS: *m/z* calcd for $C_{12}H_{14}N_4O$ $[M + Na]^+$: 253.1060; found 253.1063.

4.2.11. 1-(4-cyanophenyl)-3-[2(ethyl)butyryl]-3-methyltriazene (**1k**)

Method A was followed using 1-(4-cyanophenyl)-3-methyltriazene and 2-ethylbutyric acid. The final mixture was purified by column chromatography (methylene chloride) to yield the product as a yellow oil (yield 38.0%); ^{1}H NMR (300 MHz, $CDCl_3$) δ 7.74 (2H, d, $J = 8.8$ Hz), 7.66 (2H, d, $J = 8.8$ Hz), 3.45–3.54 (1H, m), 3.47 (3H, s), 1.72–1.86 (2H, m), 1.55–1.69 (2H, m), 0.89 (6H, t, $J = 7.4$ Hz); ^{13}C NMR (75 MHz, $CDCl_3$) δ 178.79, 152.07, 133.49, 122.81, 118.70, 112.09, 45.65, 28.31, 25.39, 12.04. HR-ESI(+)/MS: *m/z* calcd for $C_{14}H_{18}N_4O$ $[M + Na]^+$: 281.1373; found 281.1378.

4.3. Biology

4.3.1. Cell cultures

The GL261 cell line was a kind gift from Dr. Geza Safrany, from the National Research Institute for Radiobiology and Radiohygiene, in Hungary. This cell line is representative of a carcinogen-induced mouse syngeneic glioma model, which carries point mutations in the K-ras and p53 genes [27], and has features of cancer stem cells, namely elevated expression of CD133 [28]. GL261 cells were seeded in Dulbecco's Modified Eagle Medium (DMEM) supplemented with 11 mM sodium bicarbonate,

38.9 mM glucose, 10% fetal bovine serum (FBS) and 1% penicillin/streptomycin (all from Biochrom), and maintained at 37 °C in a humidified atmosphere of 5% CO_2. Cells were plated at 5×10^4 cells/mL 24 h before treatments as previously described by us [10]. Human neuroblastoma cells SH-SY5Y (SH) were a gift from Professor Anthony Turner [29]. Cells were cultured in DMEM supplemented with 10% FBS and 2% Antibiotic/Antimycotic (AB/AM, Sigma-Aldrich, Sigma). The medium was changed every 2 days. Culture plates were coated with Poly-D-Lysine (100 μg/mL) and laminin (4 μg/mL, Gibco) before plating the cells. For the experiments, cells were seeded at a concentration of 5×10^4 cells/mL and maintained at 37 °C in a humidified atmosphere of 5% CO_2. After 24 h proliferation, differentiation into a neuronal phenotype was induced by adding retinoic acid (RA, Sigma-Aldrich) at a final concentration of 10 μM in the culture medium and maintaining cells for 7 days. RA-containing culture medium was changed every 2 days.

4.3.2. Cell treatments

Glioma cells were treated with 0.1–100 μM of the compounds **1b-k** during 48 h. Compounds **1a** and TMZ (Sigma-Aldrich) were also used for comparative purposes, as described in our previous work [10]. Taking into account the results of the cell viability assays, we selected the most efficient compounds and concentrations to be used in the subsequent analyses. SH-SY-5Y cells were also treated with the selected compounds and concentrations only, to perform cell death assays.

4.3.3. Cell viability assay by MTS

Cell viability of the GL261 cells was assessed using the cellular reduction of [3-(4,5-dimethylthiazol-2-yl)-5-(3-carboxymethoxyphenyl)-2-(4-sulfophenyl)-2H-tetrazolium] (MTS) by viable cells into an aqueous, soluble and coloured formazan product, in the presence of phenazine methosulfate (PMS). After exposure to compounds **1a-k** or TMZ, cells were incubated for 1 h at 37 °C with an MTS:PMS mixture (1:20, from stock solutions of 2 mg/mL and 0.92 mg/mL, respectively) diluted 1/10 in DMEM-F12 and the absorbance was measured at 490 nm using a PR 2100 microplate reader (Bio-Rad Laboratories). For each experiment, the mean value of absorbance obtained for non-treated cells (control) was considered as 100% of cell viability.

4.3.4. Determination of cell death by necrosis and apoptosis

GL261 glioma and SH-SY5Y-neuron cell lines were treated with TMZ or selected hybrid compounds at a concentration of 10 μM during 48 h. A phycoerythrin-conjugated annexin V (V-PE) and 7-aminoactinomycin-D (7-AAD) mixture (Guava Nexin® Reagent, Millipore, MA, USA) was used to determine the percentage of viable, early-apoptotic and late-apoptotic/necrotic cells by flow cytometry. After incubation, adherent cells were collected by trypsinization and added to the cells present in the incubation media. After centrifugation, the cell pellet was resuspended in PBS containing 1% bovine serum albumin (BSA), stained with Guava Nexin® Reagent according to manufacturer's instructions, and analyzed on a Guava easyCyte 5HT flow cytometer (Guava Nexin® Software module, Millipore). Two readings were performed for each sample.

4.3.5. Glioma cell morphological assay

GL261 glioma cells were treated with TMZ or selected hybrid compounds at a concentration of 10 μM during 48 h. After incubation, cells in coverslips were fixed with freshly prepared 4% (w/v) paraformaldehyde in PBS, permeabilized with 0.1% Triton X-100 Solution and incubated with blocking solution (10% FBS in Tween-20-Tris-buffered saline) during 30 min at room temperature. To evaluate GL261 cell morphology, cells were stained with Phalloidin (which binds F-actin with high selectivity) conjugated with Alexa Fluor-594 antibody (1:50, #A12381, Thermo Fisher Scientific). Cell nuclei were stained with Hoechst 33258 dye (blue, Sigma-Aldrich) and fluorescence was visualized using an AxioCam HR camera adapted to an AxioScope A1® microscope (Zeiss, Germany). Merged images of UV and fluorescence of ten random microscopic fields were acquired per sample using Zen 2012 (blue edition, Zeiss) software. The original magnification was 630×. For morphological characterization we used the tracing analysis in ImageJ® software (1.49 version, NIH, USA) to measure cell circularity ($4\pi \frac{Area}{Perimeter^2}$) and aspect ratio ($\frac{major\ axis}{minor\ axis}$). The average of at least 120 cells was considered for in each condition.

4.3.6. Glioma cell migration assay

GL261 glioma cells were treated with TMZ or selected hybrid compounds at a concentration of 10 μM during 48 h. After incubation, a cell migration assay was performed in a 48-well microchemotaxis Boyden chamber (#AP48, Neuro Probe) by using 8 μm diameter polycarbonate membranes with polyvinylpyrrolidone (PVP) surface. Each well of the lower chamber compartment was filled with 25 μL DMEM + EGF (10%) to induce chemotaxis. Non-treated (control) and treated cells were allowed to migrate for 6 h in a CO_2 incubator at 37 °C. After this period, cells attached to lower side of the membrane were fixed with cold methanol and stained with 10% Giemsa in PBS. Non-migrated cells on the upper side of the membrane were wiped off with a filter wiper. The rate of migration was determined by counting cells on the lower membrane surface. At least six bright field images per sample were acquired using an AxioCam 105 color camera (Zeiss) adapted to an Axioskope HBO50 microscope (Zeiss). For each experiment, at least three wells per condition were analyzed.

4.4. Incubation of 1a and 4a with 5′– GGG AGA – 3′

Compound **1a** (30 μM, 100 μM, 1 mM, 2.5 mM) was incubated with the single-stranded oligonucleotide (10 μM) in ammonium bicarbonate buffer (10 mM, pH 8.3) at 37 °C. Aliquots (50 μL) of the samples were withdrawn at regular time intervals and each mixture was extracted three times with 50 μL of ethyl acetate. Upon vortexing, the mixtures were centrifuged, at 13300 rpm for 3 min and the aqueous phase was collected for MS analysis. Experiments were carried out in triplicate.

4.5. Hydrolysis in phosphate buffered saline

Isotonic phosphate buffer (10 mM, pH 7.4, 4 mL) and ACN (1 mL) were added into a Falcon tube placed in a water bath thermostated at 37 °C. After temperature stabilization, 150 μL of stock solution of **1a-k** in ACN (10 mM) were added. Several aliquots were taken at regular times, injected and analyzed by HPLC. These experiments were carried out in duplicate.

4.6. Hydrolysis in human plasma

Human plasma from 13 healthy donors was collected in sodium heparinate, divided into 2 mL fractions and stored at −18 °C until required. Before usage, frozen samples were thawed gradually to avoid denaturation of plasma proteins. Each 2 mL aliquot of human plasma was diluted to 80% (v/v) by the addition of 0.5 mL of PBS (10 mM, pH 7.4) and the mixture was placed in a water bath thermostated at 37 °C. After temperature stabilization, 75 μL of a **1a-k** stock solution in ACN (10 mM) were added. Aliquots of 100 μL were taken at regular times and transferred to eppendorfs containing

200 μL ACN to precipitate the plasma proteins. After vortexing, followed by centrifugation at 12000 rpm for 10 min, the supernatants were collected and analyzed by HPLC. These experiments were carried out in duplicate for **1a-h** and **1k** and in triplicate for **1i-j**.

4.7. HDAC inhibition assay

HDAC inhibitory activity of *N*-acyltriazenes **1a-k** was determined using the Fluor-de-Lys HDAC activity assay kit (Enzolifesciences, BML-AK500-0001). The assay was performed according to the manufacturer's instructions. The source of HDAC enzymatic activity is a HeLa nuclear extract, provided with the kit. Compounds **1a-k** were resuspended in DMSO (20 mM) and assayed in duplicate at 100, 25 and 6.25 μM. Trichostatin A and GNX-4784 [30] were used as positive controls. The reaction was starting by adding HDAC fluorometric substrate [Boc-Lys(Ac)-AMC], which contains acetylated lysine, to the inhibitors and HeLa nuclear extract mixture. Deacetylation sensitized the substrate, and treatment with the lysine developer produced the fluorophore, and fluorescence was measured after 15 min of incubation at excitation 360 nm and emission 460 nm.

Acknowledgements

This work was supported by Fundação para a Ciência e Tecnologia (FCT, Portugal) through grants UID/00100/2013 to Centro de Química Estrutural and UID/04138/2013 to iMed.ULisboa. Joint funding from FCT and the COMPETE Program through grant SAICTPAC/0019/2015 is gratefully acknowledged. CB also thanks FCT for a PhD fellowship under the MedChemTrain program (PD/BD/128239/2016). We also acknowledge the financial support from FCT and Portugal 2020 to the National Mass Spectrometry Network (RNEM LISBOA-01-0145-FEDER-402-022125 IST).

We kindly thank S. Vultaggio and C. Mercurio from IFOM - FIRC Institute of Molecular Oncology Foundation (Milano, Italy) for the HDAC activity measurements.

Appendix A. Supplementary data

Supplementary data related to this article can be found at https://doi.org/10.1016/j.ejmech.2019.03.048.

References

[1] R.L. Siegel, K.D. Miller, A. Jemal, Cancer statistics, CA Cancer J. Clin. 66 (2016) 7–30, https://doi.org/10.3322/caac.21332.
[2] Q.T. Ostrom, H. Gittleman, P.M. de Blank, J.L. Finlay, J.G. Gurney, R. McKean-Cowdin, D.S. Stearns, J.E. Wolff, M. Liu, Y. Wolinsky, C. Kruchko, J.S. Barnholtz-Sloan, American brain tumor association adolescent and young adult primary brain and central nervous system tumors diagnosed in the United States in 2008-2012, Neuro Oncol. 18 (2016) i1–i50, https://doi.org/10.1093/neuonc/nov297.
[3] R. Stupp, W.P. Mason, M.J. van den Bent, M. Weller, B. Fisher, M.J.B. Taphoorn, K. Belanger, A.A. Brandes, C. Marosi, U. Bogdahn, J. Curschmann, R.C. Janzer, S.K. Ludwin, T. Gorlia, A. Allgeier, D. Lacombe, J.G. Cairncross, E. Eisenhauer, R.O. Mirimanoff, European organisation for Research and treatment of cancer brain tumor and radiotherapy groups, national cancer Institute of Canada clinical trials group, radiotherapy plus concomitant and adjuvant temozolomide for glioblastoma, N. Engl. J. Med. 352 (2005) 987–996, https://doi.org/10.1056/NEJMoa043330.
[4] S.S. Agarwala, J.M. Kirkwood, Temozolomide, a novel alkylating agent with activity in the central nervous system, may improve the treatment of advanced metastatic melanoma, Oncol. 5 (2000) 144–151.
[5] C.L. Moody, R.T. Wheelhouse, The medicinal chemistry of imidazotetrazine prodrugs, Pharmaceuticals (Basel) 7 (2014) 797–838, https://doi.org/10.3390/ph7070797.
[6] J. Zhang, M.F.G. Stevens, T.D. Bradshaw, Temozolomide: mechanisms of action, repair and resistance, Curr. Mol. Pharmacol. 5 (2012) 102–114.
[7] S. Berendsen, M. Broekman, T. Seute, T. Snijders, C. van Es, F. de Vos, L. Regli, P. Robe, Valproic acid for the treatment of malignant gliomas: review of the preclinical rationale and published clinical results, Expert Opin. Investig. Drugs 21 (2012) 1391–1415, https://doi.org/10.1517/13543784.2012.694425.
[8] A.V. Krauze, S.D. Myrehaug, M.G. Chang, D.J. Holdford, S. Smith, J. Shih, P.J. Tofilon, H.A. Fine, K. Camphausen, A phase 2 study of concurrent radiation therapy, temozolomide, and the histone deacetylase inhibitor valproic acid for patients with glioblastoma, Int. J. Radiat. Oncol. Biol. Phys. 92 (2015) 986–992, https://doi.org/10.1016/j.ijrobp.2015.04.038.
[9] K.A. Van Nifterik, J. Van den Berg, B.J. Slotman, M.V.M. Lafleur, P. Sminia, L.J.A. Stalpers, Valproic acid sensitizes human glioma cells for temozolomide and γ-radiation, J. Neuro Oncol. 107 (2012) 61–67, https://doi.org/10.1007/s11060-011-0725-z.
[10] R. Pinheiro, C. Braga, G. Santos, M.R. Bronze, M.J. Perry, R. Moreira, D. Brites, A.S. Falcão, Targeting gliomas: can a new alkylating hybrid compound make a difference? ACS Chem. Neurosci. 8 (2017) 50–59, https://doi.org/10.1021/acschemneuro.6b00169.
[11] T.P. Ahern, H. Fong, K. Vaughan, Open-chain nitrogen compounds. Part II. Preparation, characterization, and degradation of 1(3)-Aryl-3(1)-methyltriazenes; the effect of substituents on the reaction of diazonium salts with methylamine, Can. J. Chem. 55 (1977) 1701–1709, https://doi.org/10.1139/v77-240.
[12] S.C. Cheng, J. Iley, Synthesis of 1-aryl-3-methyltriazenes by base-promoted decomposition of 1-aryl-3-hydroxymethyl-3-methyltriazenes, J. Chem. Res. (1983) 320–321.
[13] T.T. Wager, X. Hou, P.R. Verhoest, A. Villalobos, Moving beyond rules: the development of a central nervous system multiparameter optimization (CNS MPO) approach to enable alignment of drug like properties, ACS Chem. Neurosci. 1 (2010) 435–449, https://doi.org/10.1021/cn100008c.
[14] R.L. Svec, L. Furiassi, C.G. Skibinski, T.M. Fan, G.J. Riggins, P.J. Hergenrother, Tunable stability of imidazotetrazines leads to a potent compound for glioblastoma, ACS Chem. Biol. 13 (2018) 3206–3216, https://doi.org/10.1021/acschembio.8b00864.
[15] J. Kovalevich, D. Langford, Considerations for the use of SH-SY5Y neuroblastoma cells in neurobiology, Methods Mol. Biol. 1078 (2013) 9–21, https://doi.org/10.1007/978-1-62703-640-5_2.
[16] S.P. Carey, C.M. Kraning-Rush, R.M. Williams, C.A. Reinhart-King, Biophysical control of invasive tumor cell behavior by extracellular matrix microarchitecture, Biomaterials 33 (2012) 4157–4165, https://doi.org/10.1016/j.biomaterials.2012.02.029.
[17] I. Koh, J. Cha, J. Park, J. Choi, S.-G. Kang, P. Kim, The mode and dynamics of glioblastoma cell invasion into a decellularized tissue-derived extracellular matrix-based three-dimensional tumor model, Sci. Rep. 8 (2018), https://doi.org/10.1038/s41598-018-22681-3.
[18] M.-S.I. Abaza, A.-M. Bahman, R.J. Al-Attiyah, Valproic acid, an anti-epileptic drug and a histone deacetylase inhibitor, in combination with proteasome inhibitors exerts antiproliferative, pro-apoptotic and chemosensitizing effects in human colorectal cancer cells: underlying molecular mechanisms, Int. J. Mol. Med. 34 (2014) 513–532, https://doi.org/10.3892/ijmm.2014.1795.
[19] K.M. Gilbert, A. DeLoose, J.L. Valentine, E.K. Fifer, Structure–activity relationship between carboxylic acids and T cell cycle blockade, Life Sci. 78 (2006) 2159–2165, https://doi.org/10.1016/j.lfs.2005.09.047.
[20] M. de J. Perry, E. Carvalho, E. Rosa, J. Iley, Towards an efficient prodrug of the alkylating metabolite monomethyltriazene: synthesis and stability of N-acylamino acid derivatives of triazenes, Eur. J. Med. Chem. 44 (2009) 1049–1056, https://doi.org/10.1016/J.EJMECH.2008.06.022.
[21] M.B. Kroeger Smith, L.A. Taneyhill, C.J. Michejda, R.H.J. Smith, Base sequence selectivity in the alkylation of DNA by 1,3-Dialkyl-3-acyltriazenes, Chem. Res. Toxicol. 9 (1996) 341–348, https://doi.org/10.1021/tx9500742.
[22] J.A. Hartley, W.B. Mattes, K. Vaughan, N.W. Gibson, DNA sequence specificity of guanine N7-alkylations for a series of structurally related triazenes, Carcinogenesis 9 (1988) 669–674.
[23] A.S. Monteiro, J. Almeida, G. Cabral, P. Severino, P.A. Videira, A. Sousa, R. Nunes, J.D. Pereira, A.P. Francisco, M.J. Perry, E. Mendes, Synthesis and evaluation of N-acylamino acids derivatives of triazenes. Activation by tyrosinase in human melanoma cell lines, Eur. J. Med. Chem. 70 (2013) 1–9, https://doi.org/10.1016/j.ejmech.2013.09.040.
[24] F. Delben, S. Paoletti, G. Manzini, C. Nisi, Influence of serum albumins on decomposition rates of para-substituted 1-phenyl-3-methyltriazenes and 5-(3-methyl-1-triazeno)imidazole-4-carboxamide in near physiological conditions, J. Pharm. Sci. 70 (1981) 892–897.
[25] J. Iley, R. Moreira, E. Rosa, Triazene drug metabolites. Part 10. Metal-ion catalysed decomposition of monoalkyltriazenes in ethanol solutions, J. Chem. Soc. Perkin Trans. 2 (1991) 81–86, https://doi.org/10.1039/p29910000081.
[26] Biology Data Book, second ed., Federation of American Societies for Experimental Biology, Bethesda, Maryland, 1974.
[27] T. Szatmári, K. Lumniczky, S. Désaknai, S. Trajcevski, E.J. Hídvegi, H. Hamada, G. Sáfrány, Detailed characterization of the mouse glioma 261 tumor model for experimental glioblastoma therapy, Cancer Sci. 97 (2006) 546–553, https://doi.org/10.1111/j.1349-7006.2006.00208.x.
[28] A. Wu, S. Oh, S.M. Wiesner, K. Ericson, L. Chen, W.A. Hall, P.E. Champoux, W.C. Low, J.R. Ohlfest, Persistence of CD133 $^{+}$ cells in human and mouse glioma cell lines: detailed characterization of GL261 glioma cells with cancer stem cell-like properties, Stem Cell. Dev. 17 (2008) 173–184, https://doi.org/10.1089/scd.2007.0133.
[29] N.D. Belyaev, K.A.B. Kellett, C. Beckett, N.Z. Makova, T.J. Revett, N.N. Nalivaeva,

N.M. Hooper, A.J. Turner, The transcriptionally active amyloid precursor protein (APP) intracellular domain is preferentially produced from the 695 isoform of APP in a β-Secretase-dependent pathway, J. Biol. Chem. 285 (2010) 41443–41454, https://doi.org/10.1074/jbc.M110.141390.

[30] M. Varasi, F. Thaler, A. Abate, C. Bigogno, R. Boggio, G. Carenzi, T. Cataudella, R. Dal Zuffo, M.C. Fulco, M.G. Rozio, A. Mai, G. Dondio, S. Minucci, C. Mercurio, Discovery, synthesis, and pharmacological evaluation of spiropiperidine hydroxamic acid based derivatives as structurally novel histone deacetylase (HDAC) inhibitors, J. Med. Chem. 54 (2011) 3051–3064, https://doi.org/10.1021/jm200146u.